33RD INTERNATIONAL COSMIC RAY CONFERENCE, RIO DE JANEIRO 2013
THE ASTROPARTICLE PHYSICS CONFERENCE

ICRC 2013

The ISS-CREAM Boronated Scintillator Detector

T. ANDERSON[1], D. ANGELASZEK[2], J. BAYLON[3]. M. COPLEY[2], S. COUTU[1], M. GUPTA[2], J. H. HAN[2], H. G. HUH[2], Y. S. HWANG[4], H. J. HYUN[4], H. J. KIM[4], K. C. KIM[2], K. KWASHNAK[2], M. H. LEE[2], J. T. LINK[5], L. LUTZ[2], A. MALININ[2], A. MENCHACA-ROCHA[3], J. MITCHELL[6], S. NUTTER[7], O. OFOHA[2], J. M. PARK[4], P. PATTERSON[2], E. S. SEO[2], J. WU[2], Y. S. YOON[2]

[1] *Pennsylvania State University, University Park, PA 16802 USA*
[2] *University of Maryland, College Park, MD 20740 USA*
[3] *Universidad Nacional Autonoma de Mexico, Mexico*
[4] *Kyungpook National University, South Korea*
[5] *NASA Goddard/CRESST (USRA), Greenbelt, MD 20771 USA*
[6] *NASA Goddard, Greenbelt, MD 20771 USA*
[7] *Northern Kentucky University, Highland Heights, KY 41099 USA*

tba109@psu.edu

Abstract: The Boronated Scintillator Detector (BSD) is a new detector sub-system for the future Cosmic Ray Energetics and Mass for the International Space Station (ISS-CREAM) mission. It aims to complement the instrument's tungsten calorimeter in identifying cosmic-ray electrons above 100 GeV. Such electrons are of significant scientific interest, but their identification is complicated by the overwhelmingly more abundant hadronic cosmic rays, hence making significant hadronic rejection power of paramount importance. Particle showers initiated by nuclei in the ISS-CREAM calorimeter have a profile different from an electron-induced electromagnetic cascade, and the hadron rejection power deriving from this difference can be significantly enhanced by making use of the thermal neutron activity at late (>400 ns) times relative to the start of the shower. Indeed hadron-induced showers tend to be accompanied by significantly more neutron activity than electromagnetic showers. The ISS-CREAM BSD endeavors to measure this late thermal neutron shower activity by detecting the boron capture of these thermal neutrons in a boron-loaded plastic scintillator, located underneath the calorimeter. Results from a 2012 test of this plastic scintillator in the CERN H2 beam line are discussed, and a comparison of these results is made with the performance predicted by a detailed GEANT4 simulation of the ISS-CREAM instrument.

Keywords: cosmic rays, electrons, neutrons, scintillator, International Space Station.

1 Introduction

The ISS-CREAM instrument is a re-configured version of the CREAM long-duration balloon (LDB) payload, and is scheduled for deployment to the International Space Station in 2014. The primary science goal of ISS-CREAM is to measure the energy spectrum of cosmic rays between 10^{10} eV and 10^{15} eV for each species Z = 1 (hydrogen) through Z = 26 (iron). As with heritage balloon flights, ISS-CREAM will employ a multi-layer silicon charge detector to measure cosmic ray charge magnitude and a 20-layer tungsten sampling calorimeter to measure cosmic ray energy. With the addition of three new detectors—the Top Counter Detector, the Bottom Counter Detector, and the Boronated Scintillator Detector (BSD)—ISS-CREAM will take on the new science goal of measuring the cosmic ray electron spectrum above 100 GeV. Such a measurement is of significant scientific interest, particularly because cosmic ray electrons tend to lose energy quickly via synchrotron radiation in galactic magnetic fields and inverse compton scattering on the cosmic microwave background. Thus, an excess at high energies would indicate a quite local source.

Spectral measurements of cosmic ray electrons at high energies are complicated by the fact that mis-identification of the far more abundant cosmic ray protons as candidate electrons can significantly distort results. Hence, a large hadronic rejection power is critical. As a basis for electron-hadron discrimination, ISS-CREAM's BSD uses the fact that calorimeter showers originating from hadronic cosmic rays tend to produce many more neutrons than electron-generated showers. By sampling this neutron activity, the BSD will contribute to ISS-CREAM's overall hadronic rejection power.

The BSD has completed its design phase, and the flight detector is currently under construction. The BSD's scintillator block has been beam tested at CERN, and the results of this beam test, along with a comparison of these results to preliminary predictions of a GEANT4 simulation, are presented below.

2 Neutron Detection in the BSD

Neutrons entering the boron-loaded scintillator undergo the capture process

$$^{10}B + n \rightarrow {}^{7}Li + \alpha + \gamma \qquad (1)$$

with a probability inversely proportional to neutron speed, and a time constant for capture inversely proportional to ^{10}B loading. The literature on the scintillation yield resulting from a single capture suggest that roughly 570 photons are produced with each capture [1].

The mean energy deposited in ISS-CREAM's calorimeter by showering cosmic ray hadrons is known to mimic that of cosmic ray electrons with about 1/3 of the primary hadron's energy. However, on average, hadron-induced

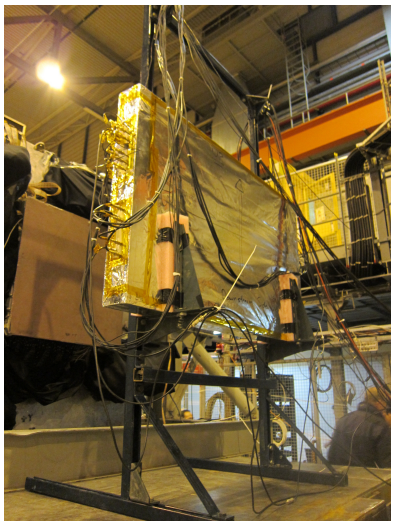

Fig. 1: The BSD is shown mounted on a unistrut frame during the CERN beam test. The ISS-CREAM pallet supporting the carbon targets and calorimeter is seen behind the BSD.

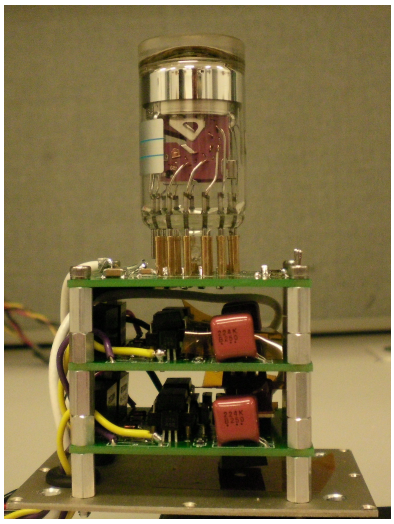

Fig. 2: A PMT assembly. The R1924A plugs in to a socketed high voltage divider board (top board). The two bottom boards switch the potential applied to dynodes 1 and 2 from -12 V during the initial calorimeter shower to their full high voltage values within 300 ns.

showers produce roughly an order of magnitude more neutrons. Once these neutrons are created, they thermalize quickly in the mass of the ISS-CREAM instrument, with total neutron activity over the course of several microseconds being measured by neutron captures in the BSD's 60 cm x 60 cm x 3.8 cm block of Eljen Technologies EJ-254 boron-loaded plastic scintillator, with 5% boron concentration by weight, with the natural ^{10}B abundance of 20%. For the BSD, neutron captures become the dominant source of photon generation beginning roughly 400 ns after the initial calorimeter shower.

3 Calibration of the ISS-CREAM BSD

In November of 2012, the BSD's flight scintillator block was calibrated along with the ISS-CREAM calorimeter in the CERN H2 beam line. This calibration provided experimental verification of the BSD's hadronic rejection strategy, made a first measurement of its expected hadronic rejection power, and provided data onto which BSD simulations can be anchored. The BSD's beam-test instrument setup is described below.

3.1 Detector Enclosure and PMTs

Figure 1 shows the BSD's detector enclosure mounted downstream of the ISS-CREAM calorimeter. The scintillator block was wrapped in 3 layers of ultra-reflective PTFE and enclosed in a light-tight box. During the beam test, the BSD detector enclosure was mounted on a unistrut frame and placed just behind the ISS-CREAM instrument.

Inside the BSD detector box, the BSD's scintillator block was viewed edge-on by 12 Hamamatsu R1924A photomultiplier tubes (PMTs), each of which was powered by a stack of three custom-designed circuit boards. (The flight unit will have 18 PMTs). The R1924A PMTs are 1-inch diameter, 10-dynode PMTs with a maximum gain of 10^7 and a spectral response ranging from 300 nm to 650 nm—a good match to EJ-254's 425 nm maximum emission wavelength.

Figure 2 shows a PMT assembly. The high voltage bias for dynodes 3 through 10 was supplied using a resistive divider with a socketed PMT connection. GEANT4 simulations predict that the early component of the calorimeter's shower creates large signals in the BSD, with each PMT being exposed to between 10^4 and 10^6 photons. Laboratory testing with the R1924A PMTs revealed that such large signals tend to induce significant PMT afterpulsing, extending up to 2 μs in duration, with amplitudes rivaling those predicted for the BSD's delayed neutron signal. In order to eliminate this afterpulsing background, two custom-designed "dynode gating boards" were incorporated into each PMT assembly's circuit board stack. These gating boards hold the potential applied to PMT dynodes 1 and 2 to -12 V during initial calorimeter showering, thereby inhibiting the injection of photoelectrons into the PMT's multiplier stage from its (grounded) photocathode. When supplied with an external dynode ON (*DON*) logic signal, the dynode gating boards switch the potentials applied to each of dynodes 1 and 2 to their normal high voltage within 300 ns. This scheme allows the BSD's PMTs to measure delayed neutron capture signals in the BSD's scintillator block, while being effectively "blind" to the large signals present during the early shower. This technique of PMT dynode gating, which has history in laser stimulated fluorescence measurements [2], was found to completely remove even the largest of early shower signals, with an ON/OFF ratio better than 10^6. For triggering purposes, two PMTs are operated at low gain, with no gating circuitry. The remaining 10 PMTs (16 in the flight unit) use the gating scheme.

3.2 Readout Electronics

A block diagram of the readout electronics used during the CERN beam test is shown in Figure 3. A NIM coincidence module was used to trigger event readout on the coincidence of two always-on PMTs, with thresholds set at the 1/2 MIP (minimum ionizing particle) level. A coincidence between these two always-on PMTs caused a NIM gate/delay generator to immediately activate the dynode ON (*DON*) logic signal. *DON* was fed into each PMT

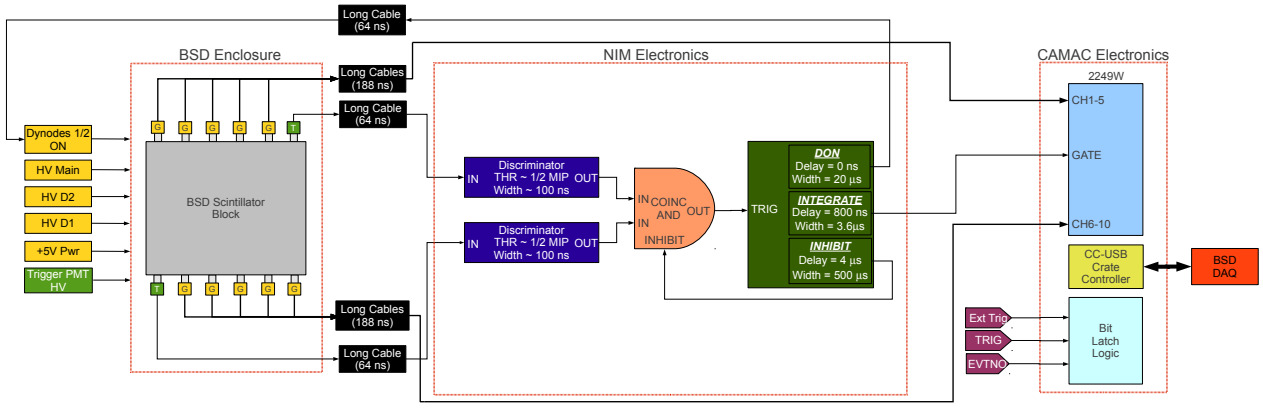

Fig. 3: A block diagram of the BSD CERN readout electronics.

dynode gating board, thereby initiating the switching-ON of the high voltage to dynodes 1 and 2 for the 10 gated PMTs. Each gated PMT anode signal was fed into a CAMAC 2249W charge integrating ADC module. A second gate/delay generator fired the *INTEGRATE* signal, which caused the 2249W to integrate the total charge from each gated PMT anode 900 ns–4500 ns after the passage of the initial particle. Re-triggering of the BSD was inhibited for 500 μs after the end of each readout.

4 Beam Test Data and Analysis

The H2 beam line was tuned for electrons at energies of 75 GeV, 100 GeV, 125 GeV, 150 GeV, and 175 GeV. Protons were unavailable at the time of this beam test. However, for the purpose of characterizing and calibrating the BSD, pions provide a good hadronic substitute, as they are known to create calorimeter showers similar to those generated by protons. The H2 beam line was also tuned for pions at energies of 250 GeV, 300 GeV, and 350 GeV.

Offline analysis of the data collected from these beam runs proceeded as follows. The 10 pedestal-subtracted and gain-normalized gated BSD PMT signals were summed, and the resulting quantity was taken as the BSD's delayed neutron activity signal. Likewise, each of the scintillating fiber ribbons in the calorimeter were pedestal subtracted, and the five ribbons on to which the beam was centered were summed over all calorimeter layers. The resulting sum was taken as the energy deposit in the calorimeter.

A quality cut was applied requiring greater than 40 MeV energy deposit in six consecutive calorimeter layers. This cut had the important effects of both simulating flight trigger conditions and selecting a pure sample of electrons and pions for analysis.

Figure 4 shows the resulting energy deposit distributions for electrons and pions in both the BSD and the calorimeter. The BSD's ability to distinguish electrons from hadrons is immediately clear. Even for a broad range of calorimeter signal values, the BSD's electron distribution tends to cluster at lower values of BSD signal than the pion distribution. As will be seen, these differences sharpen even more when the calorimeter's signal range is limited to emulate an energy range selection of the sort that will be carried out with flight data.

5 Comparison with Simulation

A GEANT4 monte carlo of the BSD's beam test conditions is currently under development, but preliminary comparisons with data are possible. Neutron physics is simulated via the QGSP_BIC_HP physics list, which incorporates the gamut of both elastic and inelastic neutron interaction processes.

Figure 5 compares the measured BSD signal distributions from the 150 GeV electron and 350 GeV pion runs in the CERN beam test (red), with the monte carlo's predicted distributions (blue). The BSD's monte carlo signal is derived directly from the total number of BSD neutron captures, with simple Poissonian smearing added to account for variations in photon propagation. Neutron capture peaks are visible, indicating that an improved accounting of resolution and background effects needs to be implemented in the simulations.

A single normalization factor was chosen for both electrons and pions so as to best align simulations with CERN data. Work to refine and match simulation results to beam test data is active and ongoing, including laboratory tests with a ^{252}Cf neutron source and cross checks of GEANT4's neutron physics model.

6 Hadronic Rejection Power

An analysis was performed on events with calorimeter total energy deposit values between 6000 counts (roughly 670 MeV total energy deposit) and 9000 counts (roughly 1 GeV total energy deposit). This corresponds to overlapping calorimeter energy deposit distributions for electron runs 100 GeV–125 GeV and pion runs 250 GeV–350 GeV.

For the purpose of deriving rejection power, the parameter E_{frac} is defined as

$$E_{frac} = \frac{\text{(BSD Delayed Neutron Signal)}}{\text{(Calorimeter Energy Deposit)}} \qquad (2)$$

A plot of E_{frac} in a specific range of calorimeter energy deposit is shown in Figure 6, with electrons shown in red and pions shown in blue. Clearly, the majority of pions fall well outside of the range of E_{frac} values for electrons, most of which lie below $E_{frac} = 0.1$. Thus, in choosing candidate electron populations for spectral studies, a higher

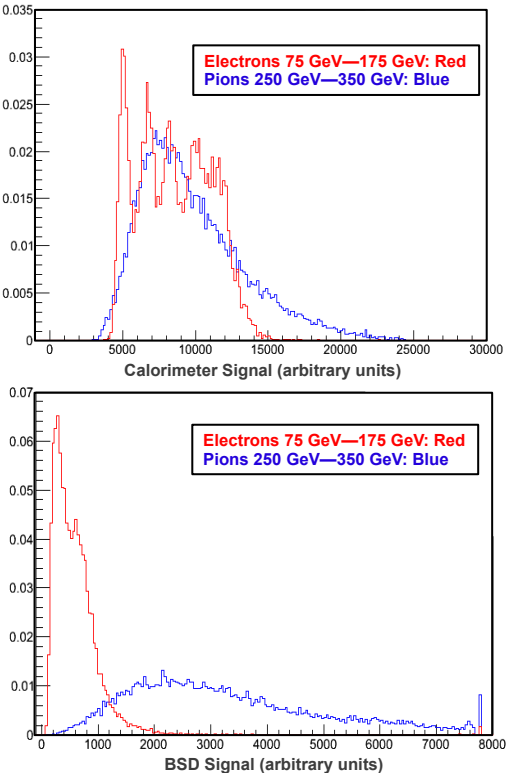

Fig. 4: Calorimeter (top) and BSD (bottom) signals for 75 GeV, 100 GeV, 125 GeV, 150 GeV, and 175 GeV electron runs (red) and 250 GeV, 300 GeV, and 350 GeV pion runs (blue). Histograms are normalized by total number of counts.

purity of electrons can be exchanged for a reduced detection efficiency by reducing the maximum allowable value of E_{frac}.

Below a given value of E_{frac}, hadronic rejection power for the BSD was defined as

$$\text{Rej. Power} = \frac{(\text{Fraction of Electrons Accepted})}{(\text{Fraction of Hadrons Not Rejected})} \quad (3)$$

Figure 7 shows a plot of rejection power versus electron acceptance derived by gradually raising the maximum allowable value of E_{frac} in Figure 6. Error bars are statistical only. Here, the rejection power using only the BSD and the total energy deposit in the calorimeter is near 140 at 50% electron acceptance, which was the BSD target design performance specification. Rejection power from other handles on electron/hadron discrimination (*e.g.* shower shape) will combine with the BSD's neutron detection to create ISS-CREAM's overall planned rejection power of at least 10^4.

Acknowledgment: The authors thank the NASA Wallops Flight Facility, for project management and engineering support, and CERN for the availability of test beams. This work is supported in the U.S. by NASA grants NNX11AC52G, NNX08AC15G, NNX08AC16G and their predecessor grants, as well as directed RTOP funds to the NASA Goddard Space Flight Center. It is supported in Korea by National Space Laboratory Program of National Research Foundation.

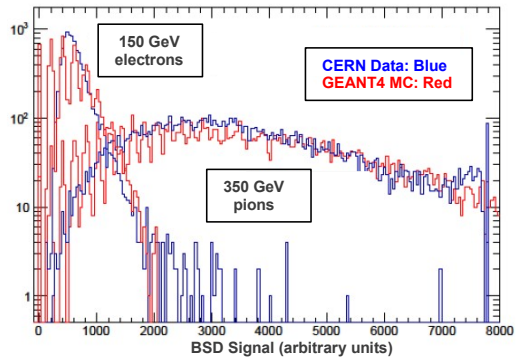

Fig. 5: Comparison of CERN data (red) with the GEANT4 simulation (blue). The small-scale structure in the simulated distributions results from the fact that sufficient smearing has not yet been fully accounted for and is not physically meaningful.

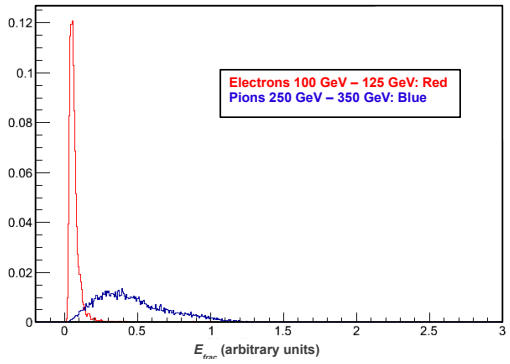

Fig. 6: E_{frac} distributions for 100 GeV–125 GeV electrons (red) and 250 GeV–350 GeV pions (blue). Histograms are normalized by total number of counts.

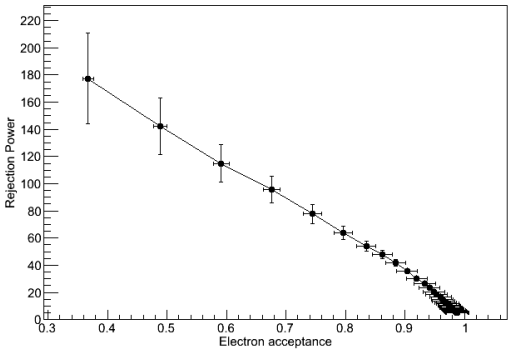

Fig. 7: Rejection power versus electron acceptance for 100 GeV–125 GeV electrons and 250 GeV–350 GeV pions.

References

[1] D. M. Drake, W. C. Feldman, and C. Hurlbut, Nuclear Instruments and Methods in Physics Research, A247 (1986) 576-582.
[2] F. De Martini and K. Wacks, The Review of Scientific Instruments, 38 (1976) 886-888.